Available at: http://www.ictp.it/~pub_off IC/2006/146

United Nations Educational, Scientific and Cultural Organization
and
International Atomic Energy Agency

THE ABDUS SALAM INTERNATIONAL CENTRE FOR THEORETICAL PHYSICS

CHARACTERIZATION OF THE DYNAMIC RESPONSE OF STRUCTURES TO DAMAGING PULSE-TYPE NEAR-FAULT GROUND MOTIONS

Fabrizio Mollaioli, Silvia Bruno, Luis D. Decanini
Dipartimento di Ingegneria Strutturale e Geotecnica, Università di Roma "La Sapienza", Roma, Italy

and

Giuliano F. Panza
Dipartimento di Scienze della Terra, Università di Trieste, Trieste, Italy
and
The Abdus Salam International Centre for Theoretical Physics, Trieste, Italy.

MIRAMARE – TRIESTE

December 2006

Abstract

The presence of long-period pulses in near-fault records can be considered as an important factor in causing damage due to the transmission of large amounts of energy to the structures in a very short time. Under such circumstances high-energy dissipation demands usually occur, which are likely to concentrate in the weakest parts of the structure. The maximum nonlinear response or collapse often happens at the onset of directivity pulse and fling, and this time is not predicted by the natural structural vibration periods. Nonlinear response leading to collapse may in most cases occur only during one large amplitude pulse of displacement. From the study of the response of both linear and nonlinear SDOF systems, the effects of these distinctive long-period pulses have been assessed by means of: (i) synthetic parameters directly derived from the strong ground motion records, and (ii) elastic and inelastic spectra of both conventional and energy-based seismic demand parameters. SDOF systems have first been subjected to records obtained during recent earthquakes in near-fault areas in forward directivity conditions. The results indicate that long duration pulses strongly affect the inelastic response, with very high energy and displacement demands which may be several times larger than the limit values specified by the majority of codes. In addition, from the recognition of the fundamental importance of velocity and energy-based parameters in the characterization of near-fault signals, idealized pulses equivalent to near-fault signals have been defined on account of such parameters. Equivalent pulses are capable of representing the salient observed features of the response to near-fault recorded ground motions.

1. Introduction

The increased availability of recorded ground motions consequent to recent seismic events such as Northridge 1994, Kobe 1995, Turkey and Taiwan 1999, suggests that the dynamic characteristics of ground shaking can significantly vary as a function of the location of the recording station with respect to the fault and the evolution of the rupture process, particularly when the recording station itself is placed in the near-fault region. It is well known that, under certain conditions, earthquake ground

motions can consist of a limited number of distinct velocity and displacement long duration pulses.

Near-fault ground motions often contain large long-period (2–5 s) wave pulses. They can be generated by (i) constructive interference of the radiated waves due to directivity of the fault rupture, or (ii) movement of the ground associated with the permanent geodetic offset. To keep these two effects separate, the terms "directivity pulse" and "fling-step" are used for the rupture directivity and elastic rebound effects, respectively [1].

Rupture directivity effects occur when the fault ruptures toward the site and the slip direction (on the fault plane) is aligned with the rupture direction [2]. The consequent pulse is strongest on the component of motion perpendicular to the strike of the fault (fault-normal component). Fling-step ground motion occurs close to a ruptured fault with significant surface offset. It is limited to the ground displacement component parallel to the slip direction. The rupture directivity effect will be strongest on the fault normal component at a location up-dip from the hypocenter. The fling step will be observed on the horizontal component perpendicular to the strike of the fault. Consequently, for dip-slip faults, directivity-pulse effects and fling-step effects can be combined on the same component.

In earthquakes with magnitude above 6.5 the above effects can be very large [3]. For example, the horizontal velocity recordings of the Pacoima station in the 1971 San Fernando, California earthquake, had a maximum amplitude of 113 cm/s, and consisted predominantly of horizontally polarized SH wave motion with relatively long period, of about 2–3 s [4]. The ground motion damage potential in near-fault conditions is strongly influenced by the fault mechanism and by rupture propagation and radiation pattern effects [5]. We will concentrate here on directivity pulses, while the analysis of flings will be the subject of a forthcoming study.

The propagation of the fault rupture toward a site, at a velocity that is almost as large as the shear wave velocity, causes most of the seismic energy to arrive coherently in relatively large long-period pulses of motion [6, 7]. Such effect is more pronounced on displacement and velocity time histories than on accelerations. In the case of backward directivity, occurring when the rupture propagates away from the site, relatively lower amplitudes and longer duration characterize in general the corresponding motion. Long-period pulses due to near-fault rupture directivity are produced by the superposition of waves radiated from asperities of the fault. The degree of superposition depends on the station location with respect to the fault, and is affected by the mechanical characteristics of the propagation media. The limited number of records from the near-fault region does not allow characterizing the influence of the seismotectonic environment completely; therefore reliance should be placed on realistic seismological simulations in order to quantify the pulse effects adequately. The directivity itself is a well-known phenomenon in seismology [5–7, 8–14], yet only recently the impact of the directivity pulse has been considered in a limited number of seismic codes [15, 16].

The presence of severe, long duration pulses in near-field ground motions gives rise to considerable velocity and displacement demands, and can be therefore considered as a key factor in causing damage. This phenomenon entails the transmission, into the structure, of large amounts of energy, which should be dissipated in a short time, so that high-energy dissipation demands occur. This behavior is characterized

by one or two large inelastic excursions with few reversals, usually concentrated in the weakest parts of the structure, such as soft stories and any other zone where sharp changes in strength or stiffness occur. On the other hand high frequency, harmonic motions, typical of far-field records, generally require a continuum dissipation of energy over a relatively long time, with numerous yield reversals. Therefore, while the total input energy corresponding to long duration ground motion pulses (i.e., pulses of low to medium frequency) can reach considerable values, even though the seismic intensity is not particularly significant, high frequency motions do not produce severe damage, since their high spectral accelerations correspond to moderate energy imparted effectively to structures.

Recent concern about damage potential of near-field ground motion has led to considerable interest in the nature of this kind of motion and its impact on structural performance [13]. The influence of large velocity pulses on the structural response was first pointed out by Bertero *et al.* [8, 9]. In particular, in the analysis of the damage suffered by the Olive View Hospital, a few kilometers down the rupture surface of the 1971 San Fernando Earthquake, it was suggested that the significant nonlinear structural behavior would probably have occurred during the response to the relatively long duration pulse highlighted by the Pacoima Dam record [9].

The misleading notion of scaling the earthquake intensity near to a fault by a peak ground acceleration value, since it is normally associated to waves of relatively high frequency, had been previously discussed [17]. From the point of view of the characterization of the damage potential, after the 1979 Imperial Valley earthquake Anderson and Bertero [18] identified the incremental velocity, defined as the area under the largest acceleration pulse, as a significant parameter in the characterization of the severity of near-fault shakings. Moreover, they pointed out that long duration acceleration pulses are especially damaging if the width of the pulse is large compared with the natural period of the structure. These concepts were reasserted by Naeim [19] and Decanini and Mollaioli [20]. Several other studies highlighted the importance of pulse-type motions with the analysis of elastic and inelastic SDOF and MDOF systems [21–28].

Recently, the importance of assessing near-fault effects has led several authors to demonstrate that near-fault records with forward directivity can be represented by equivalent pulses defined on the basis of a limited number of ground motion parameters [3, 13, 14, 19, 29–34]. On recognizing that the intensity and distribution of the seismic energy demand depend upon the duration of the pulses, in Decanini *et al.* [35] the significance of energy-based parameters in the characterization of the seismic demand of structures subject to near-fault pulses has been emphasized, and some relationships between energy and displacement demands have been suggested.

In response to the realization of the importance of near-fault motions on structural performance, in a first part of this paper the characterization of the damage potential of long duration pulses is described. Then, the findings from a comprehensive study of about 250 near-fault ground motions recorded during 27 earthquakes, are presented. From the study of the response of SDOF systems, having nonlinear behavior, the effect of long-period pulses derived from records obtained during recent earthquakes is analyzed by means of (i) synthetic parameters directly derived from the strong ground motion records, such as peak ground acceleration,

peak ground velocity, incremental velocity, etc., and (ii) elastic and inelastic spectra of input energy, hysteretic energy, displacement and seismic resistance.

In a subsequent stage, a simplified parameterization of pulse-type forward directivity ground motions is illustrated. Starting from an energy-based characterization of the damage potential, a series of response quantities, namely the incremental velocity (indicated as one of the most important factors influencing the maximum inelastic response of structures subject to near-fault ground motions), the area enclosed by the input energy spectra and the pulse duration, are used in order to obtain a simplified representation of pulse-type motions by means of idealized pulses defined on the basis of trigonometric functions. With the aim of verifying whether the response quantities to idealized, severe pulse-type ground motions can be regarded as adequately representative of those evaluated using recorded ground motions, energy and displacement demand is computed inputting to elastic and inelastic SDOF and MDOF systems a series of idealized pulses equivalent to near-fault ground motions.

2. Damage Potential of Long Duration Pulses

As a general rule, the current linear-elastic response spectra do not provide sufficient information to account for the energy transmission mechanisms attributable to the presence of long duration pulses in near-field ground motions. In this context, even the opportunity of adopting inelastic response spectra derived from the elastic response spectra is questionable, since the excitations that induce the maximum response in elastic and inelastic systems are different in kind. It is therefore necessary to complement such information with data on the duration of strong ground motion and the number, sequence and characteristics of intense, relatively long acceleration pulses, associated with large velocity increments.

A comparison of the different effects produced by impulsive and harmonic excitations has been illustrated in Bertero *et al.* [8] and Mollaioli and Decanini [36] with a series of analyses on SDOF elastic and inelastic systems subject to simple idealized ground motion. Again in the present paper the study of the mechanical behavior of SDOF elastic and inelastic systems has been carried out in order to highlight the importance of considering, in the assessment of the effective damage potential of earthquakes, the mutual relations between different types of ground motion and the structural performance. The effects of both high frequency and long-period pulses have been investigated by computing strength, energy and displacement demand, underlining the significance of energy-based parameters in the characterization of the seismic demand of structural systems subject to such pulses.

Two simple idealized ground motions have been considered, both made up of sinusoidal motions of different frequency and duration, with null initial acceleration, velocity and displacement, and consisting in a single pulse of duration, T_{p}, equal to 1.0 s, followed by a harmonic motion of duration, d_{hm}, equal to 2.0 s and period, T_{hm}, equal to 0.2 s. The first, denoted as Type 1, is characterized by the fact that both the single pulse and the harmonic motion have the relative maximum acceleration equal to $0.35\,g$, $PGA_p = PGA_{hm} = 0.35\,g$, while in the second, denoted as Type 2, the relative acceleration maximum of the single pulse is two thirds of that of the

harmonic motion, $PGA_p = 0.35\,g = \frac{2}{3}PGA_{hm}$. The response of SDOF systems in terms of displacement demand, δ, has been analyzed with reference to a linear elastic and an elasto-plastic model. The results presented herein refer to oscillators with damping coefficient, ξ, equal to 5% of critical, and yield strength, C_y, equal to $0.15\,g$ and $0.2\,g$. The natural period, T, has been set equal to 0.2 s, i.e., coinciding with the period of the harmonic excitation, T_{hm}, and to 0.4 s, i.e., greater than T_{hm} but still far from the duration of the single pulse. From the inspection of the curves reported in Figure 1, the effects of long duration pulses on the response of oscillators beyond the elastic threshold are clearly visible and it appears that, for a given system, the definition of a critical ground motion strongly depends on the constitutive law adopted for that system.

As expected, for linear-elastic systems, the critical dynamic excitation is that of periodic type with frequency equal to that of the system (i.e., the harmonic part of both types 1 and 2 idealized motions, with $T_{hm} = 0.2$ s), since it induces a resonance phenomenon in the oscillators with natural period T equal to 0.2 s (Figure 1a and b, top). On the contrary, long duration pulses may become critical for inelastic system, especially in the case of oscillators with yielding resistance, R_y, equal or less than the inertial force corresponding to the effective ground acceleration of the pulse, i.e., $R_y \leqslant m\ddot{u}_{g,max}$ or $C_y \leqslant \ddot{u}_{g,max}/g$, where m is the mass of the system and $\ddot{u}_{g,max}$ is the maximum ground acceleration. Moreover, the displacement demand increases as the natural period of the oscillators approaches the duration of the single pulse (Figure 1a and b, bottom). In the case of elasto-plastic systems, the presence of periodic, high frequency acceleration pulses in the ground motion only contributes to building the response of the system up to its yielding threshold.

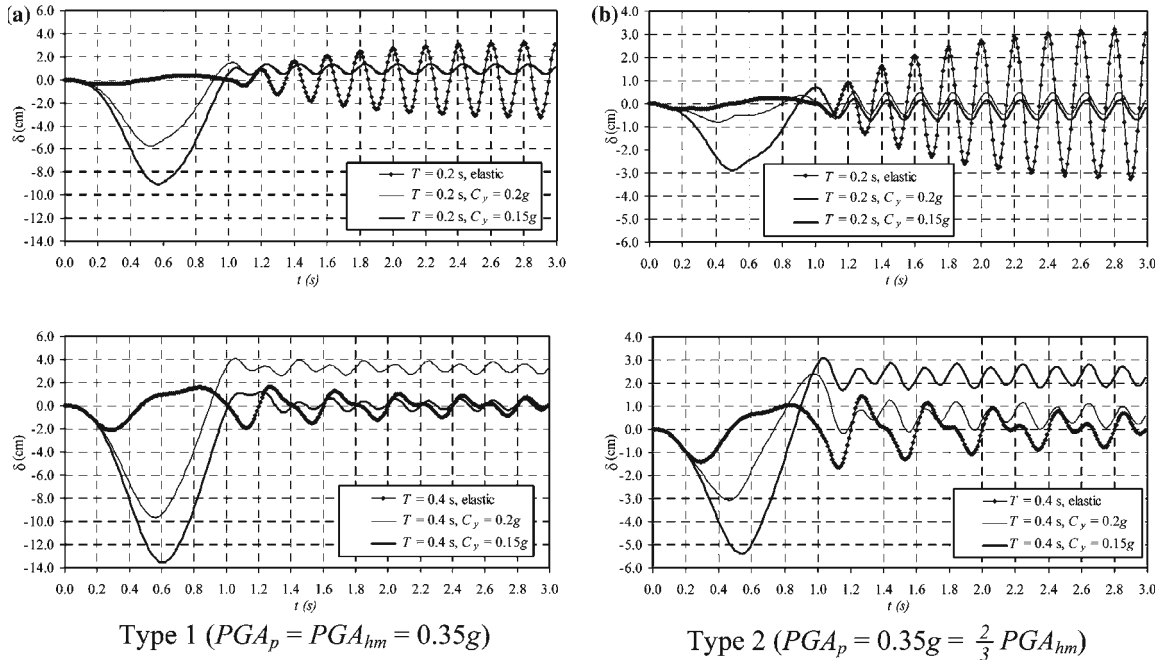

Figure 1. Displacement demand, δ, for SDOF systems subject to idealized near-fault ground motions (pulse of duration $T_p = 1.0$ s, followed by a harmonic motion of duration $d_{hm} = 2.0$ s and period $T_{hm} = 0.2$ s).

Once the system begins to yield, the phenomenon of response amplification due to resonance is mitigated, since the energy dissipated through even small inelastic deformations is associated to large values of ξ [8]. Therefore, large inelastic deformations do not occur during yielding reversal induced by periodic short pulses. Actually, the number and amplitude of these reversals are not sufficient to give rise to low cycle fatigue phenomena, since the amount of inelastic strain, developed in each excursion during an earthquake, is usually so small that the number of cycles necessary to cause collapse would exceed the number of cycles which may occur in the longest strong motions of actual earthquakes. The high displacement demands, imposed by the long duration pulse, suggest that the effective acceleration values of long duration pulses, generally coincident with the peak ground acceleration, PGA, are greater than those relevant to high frequency excitations, even when the former are characterized by lower values of PGA than the latter.

The results shown in Figure 1 confirm that, while the maximum linear-elastic response of a structural system is usually controlled by the resonance phenomenon, considerably larger deformations can be induced by the presence of just one, long pulse with an effective acceleration even slightly greater than that corresponding to the yielding strength of the structure. It is also evident from Figure 1 that, the larger the intensity of the effective acceleration of a pulse with respect to the yielding strength of the system, the larger the amount of inelastic deformations that will develop; furthermore, while high frequency motions are critical essentially for elastic systems with fundamental period close to the resonance period, long duration pulses appear to be critical for structures with fundamental periods laying within a significantly wider interval. Actually, according to Bertero *et al.* [8], the presence of repeated severe long acceleration pulses can produce a sufficient amount of cumulative damage to give rise to one or a combination of two types of failure, respectively known as low cycle fatigue and incremental collapse or crawling. In Bertero *et al.* [8] it is emphasized the advise to design structures against that type of incremental collapse (between the two listed above) which appears to constitute the critical failure. Similar conclusions may be drawn from Figure 2, that shows, for SDOF systems with $\xi = 5\%$, $T = 0.4\,\mathrm{s}$, and C_y equal to $0.15\,g$ and $0.2\,g$, the demand (per unit of mass) in terms of input energy, E_I, and hysteretic energy, E_H, according to the definition given in [37]. The totality of the energy demand is concentrated in the time interval corresponding to the long duration pulse. This time interval is not long enough for the structure to efficiently utilize the structural damping; consequently, most of the energy is dissipated through hysteresis, which implies the development of structural damage.

On recognizing that the intensity and distribution of the seismic input energy depend upon the duration of the velocity pulses, Decanini *et al.* [35] emphasized the significance of energy-based parameters in the characterization of the seismic demand of structural systems subjected to near-fault motions. In addition, they proposed some relationships between energy and displacement demands, both parameters being involved in the damage potential evaluation of near-fault ground motions. Among the various parameters directly derivable from ground motions time histories, the incremental velocity constitutes a particularly adequate index of the earthquake destructive capacity [18–20]. Pointing to the prominent role of energy spectral parameters in the description of the seismic damage potential, reference is made throughout

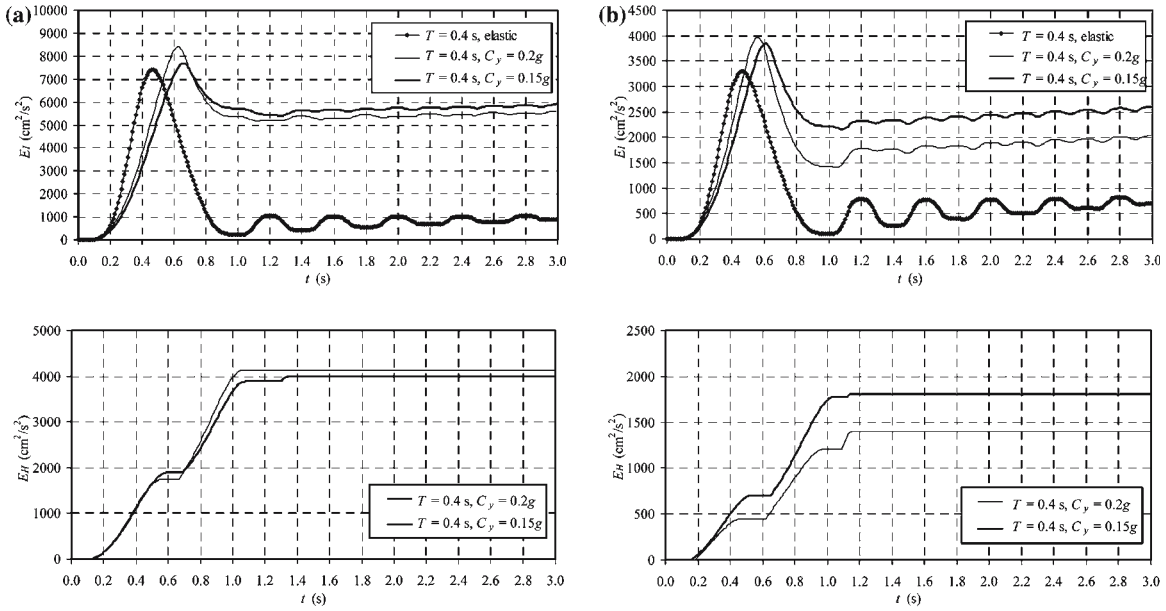

Figure 2. Energy demand for SDOF systems subject to idealized near-fault ground motions (pulse of duration T_p=1.0 s, followed by a harmonic motion of duration d_{hm}=2.0 s and period T_{hm}=0.2 s).

this study to the seismic input energy, E_I, and to the seismic hazard energy factor, AE_I, introduced in Decanini and Mollaioli [38] and defined as the area enclosed by the elastic input energy spectrum in the interval of periods between 0.05 s and 4.0 s,

$$AE_I = \int_{0.05\text{s}}^{4.0\text{s}} E_I\,(\xi = 5\%,\ T)dT \tag{1}$$

where ξ is the damping coefficient and T is the period. The seismic hazard energy factor can also be interpreted as the energy version of the Housner Intensity, I_H [39],

$$I_H = \int_{0.1\text{s}}^{2.5\text{s}} S_{PV}\,(\xi = 2\%,\ T)dT \tag{2}$$

where S_{PV} is the pseudovelocity spectrum. However, the pseudovelocity spectrum provides a lower bound to the input energy equivalent velocity spectrum, V_{E_I}, obtained as $V_{E_I} = \sqrt{2E_I}$ [40]. Unlike the peak energy spectral ordinate $(E_I)_{max}$, which generally corresponds to a narrow band of frequencies, the quantity AE_I has the advantage of taking the global energy structural response into account and it is the most statistically stable parameter in energetic analysis. Finally, as it will be shown in the next sections, the seismic hazard energy factor, AE_I, correlates quite well with the incremental velocity.

3. Analysis of the Response to some Representative Near-Fault Records

Near-fault records obtained during the 1979 Imperial Valley Earthquake contain severe velocity and displacement pulses. In Figure 3a the location of the recording stations

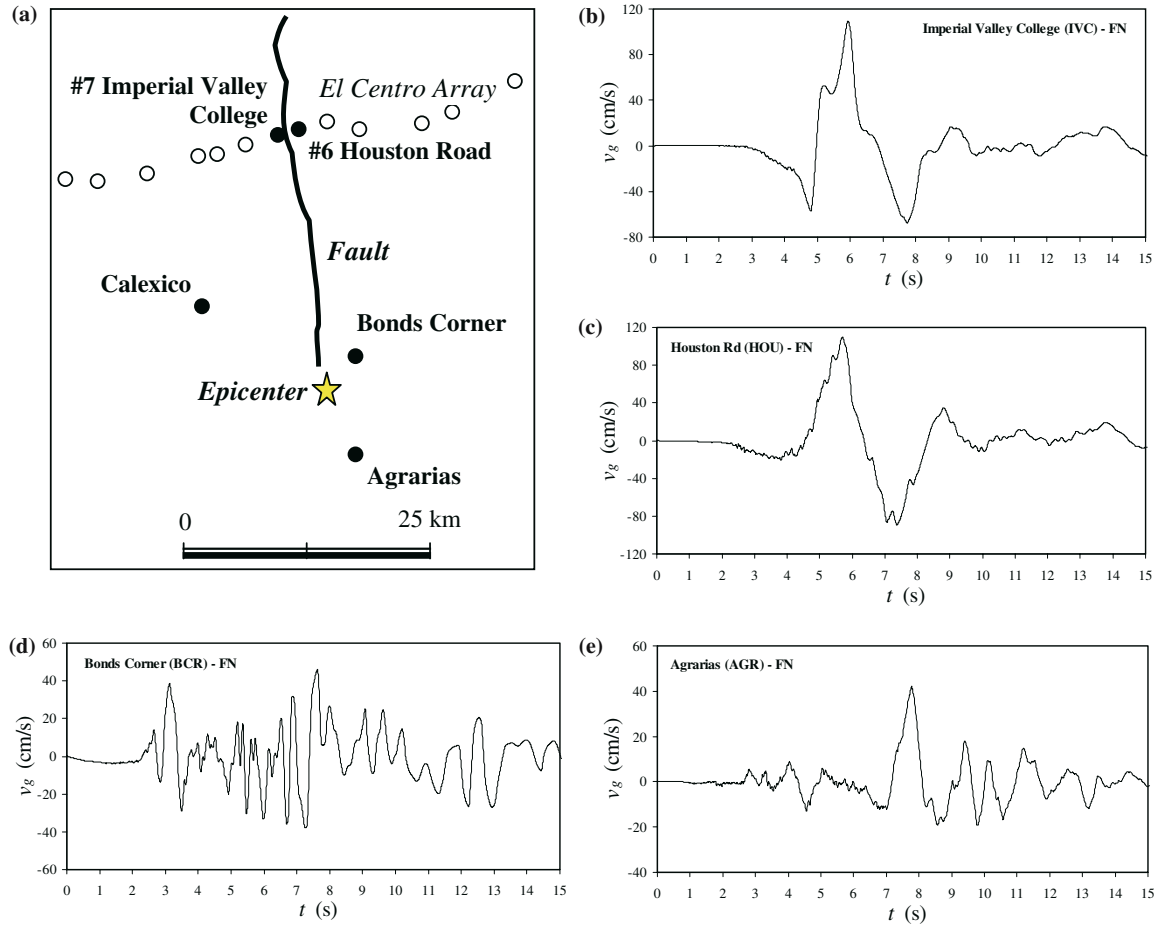

Figure 3. 1979 Imperial Valley Earthquake: recording stations (a); ground velocity time histories recorded in directivity conditions (b, c, d, e).

considered in the present study with respect to the causative fault is shown. Since the strike-slip fault rupture progressed toward the El Centro Array, #7 Imperial Valley College Station (IVC) and #6 Houston Road Station (HOU) can be considered in forward directivity conditions, while Agrarias Station (AGR) is in backward directivity conditions. Due to the proximity to the epicenter, Bonds Corner Station (BCR) can be regarded as in neutral position. Records from Calexico Station (CXO), which are not affected by directivity effects, were also considered for mere comparison purposes.

The velocity, v_g, time histories shown in Figure 3b–e for the fault-normal (FN) components of the four stations affected by directivity indicate the presence of long duration pulses, particularly in forward directivity conditions. In fact, at the beginning of the velocity time histories of IVC Station and Houston Road Station, pulses of duration, T_p, equal to approximately 3.7 s are detected.

The elastic spectra of input energy, E_I, and the seismic coefficient, C_y, are shown in Figure 4. The spectral ordinates of E_I reach the maximum at periods T close to the value of T_p. Since the energy demand, E_I, attains the largest values in the long-period region (i.e., for $2.5 \leqslant T \leqslant 4.0$ s approximately, at least for IVC FN and HOU FN curves), on reckoning that the seismic coefficient spectral ordinates keep equal to approximately $0.5\,g$ in the same period range, it can be concluded that critical

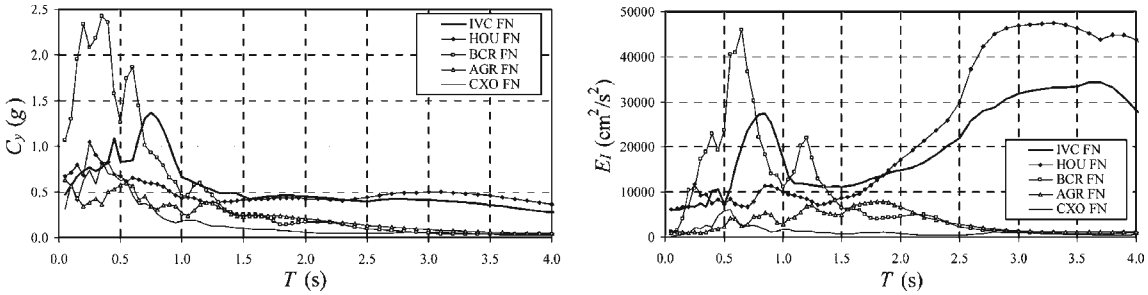

Figure 4. 1979 Imperial Valley Earthquake: seismic coefficient and input energy elastic spectra.

conditions may develop for a wide class of structures, actually designed to ensure lower values of the seismic coefficient, C_y. In fact, as shown in Figure 4, the general features that make near-fault signals in forward directivity conditions particularly critical for structures are: (a) the period range, within which the energy demand is maximum, is wider than that characterizing other type of signals, such as those recorded at Calexico, Bonds Corner and Agrarias stations; (b) the strength demand keeps considerably high in the same period range.

In Table 1 the values of peak ground acceleration, *PGA*, peak ground velocity, *PGV*, incremental velocity, *IV*, seismic hazard energy factor, AE_I, and peak energy spectral ordinate, $(E_I)_{max}$, relevant to the fault-normal, FN, and fault-parallel, FP, components of the ground motions considered are reported.

In the records IVC and HOU, velocity and energy parameters appear to be more indicative quantities of the effects of forward directivity on the FN components than *PGA*. In fact, while the ratios of the values relevant to the FN component to those relevant to the FP component are about 2–3 for the former, they are close to the unity for the latter. This result can also be observed in the inelastic case, for values of the ductility ratio, μ, equal to 2 and 4. Such circumstances do not occur for the remaining signals considered, recorded in backward directivity conditions or outside the near-field. The FN components of HOU and IVC are significantly different from the other records both in terms of energy and velocity demands.

Near-fault records obtained during the 1992 Landers, California Earthquake offer another clear example of forward and backward directivity effects. This event, one of the largest in California since 1952 with magnitude $M_w = 7.3$, was caused by a right-lateral strike-slip fault with a slip length of about 70 km. The near-fault stations activated during the earthquake were located in different position with respect to the fault rupture directivity. In particular, the Lucerne Valley Station (LV) was within a distance of 2 km from the fault trace, near the end of the fault segment that ruptured, in a forward directivity position, while the Joshua Tree Station (JT), located also in the near-field, was at a distance of about 8 km from the surface projection of the rupture, in a backward directivity position. Even though both stations were close to the fault, the damage potential exhibited by the corresponding records is very different. The FN component of Lucerne Valley record presents, in the velocity trace, a severe long duration pulse of about 4.5–4.8 s (Figure 5), which is not readily visible in the acceleration trace.

Table 1. 1979 Imperial Valley Earthquake: ground motions parameters

	#6 Houston Rd			#7 IVC			Bonds corner			Agrarias			Calexico		
	FN	FP	FN/FP	FN	FP	FN/FP	FN	FP	FN/FP	FN	FP	FN/FP	FN	FP	FN/FP
PGA (cm/s^2)	431	403	1.1	454	331	1.4	760	577	1.3	216	363	0.6	270	197	1.4
PGV (cm/s)	110	65	1.7	109	48	2.3	46	45	1.0	42	35	1.2	18	16	1.1
IV (cm/s)	199	62	3.2	177	65	2.7	84	77	1.1	53	44	1.2	29	23	1.3
$AE_{I,elastic}$ (cm^2/s)	100935	44250	2.3	83952	25882	3.2	33406	24216	1.4	13305	7888	1.7	4667	4875	1.0
$AE_{I,\mu=2}$ (cm^2/s)	83902	36316	2.3	63589	20630	3.1	30285	21592	1.4	11221	8538	1.3	4469	4528	1.0
$AE_{I,\mu=4}$ (cm^2/s)	66882	27646	2.4	54444	16239	3.4	25876	18349	1.4	8912	6748	1.3	3873	4199	0.9
$(E_I)_{max,elastic}$ (cm^2/s^2)	50557	23477	2.2	36342	13589	2.7	45462	29706	1.5	10115	6030	1.7	6151	3326	1.8
$(E_I)_{max,\ \mu=2}$ (cm^2/s^2)	36007	16449	2.2	21383	10893	2.0	36596	24618	1.5	7236	4955	1.5	5489	2834	1.9
$(E_I)_{max,\ \mu=4}$ (cm^2/s^2)	31710	12029	2.6	17300	7907	2.2	26436	20162	1.3	6300	3789	1.7	4260	2274	1.9

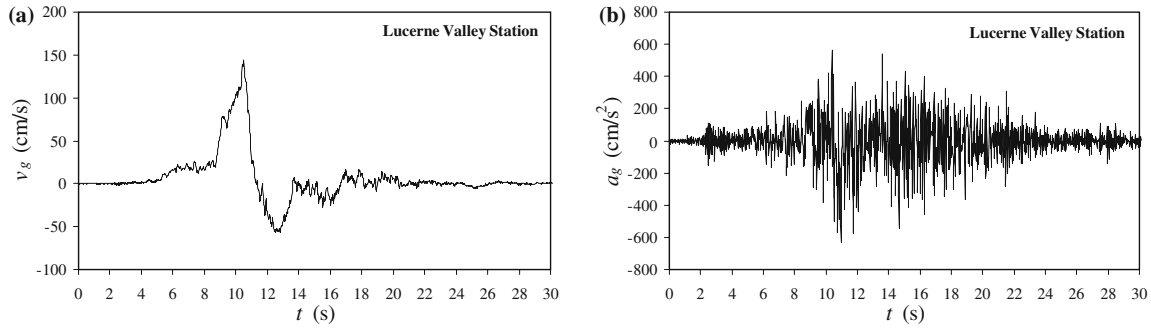

Figure 5. 1992 Landers Earthquake: ground velocity (a) and acceleration (b) time histories recorded in forward directivity conditions (FN components).

Table 2. 1992 Landers Earthquake: ground motions parameters

	Lucerne Valley (LV)			Joshua Tree (JT)			
	FN	FP	FN/FP	FN	FP	FN/FP	FN_{LV}/FN_{JT}
PGA (cm/s^2)	713	774	0.9	278	268	1.0	2.6
PGV (cm/s)	146	33	4.4	42.7	27.1	1.6	3.4
IV (cm/s)	200	31	6.5	62	44	1.4	3.2
$AE_{I,\ elastic}$ (cm^2/s)	64963	10736	6.1	36809	19579	1.9	1.8
$AE_{I,\ \mu=2}$ (cm^2/s)	63542	9225	6.9	32861	18344	1.8	1.9
$AE_{I,\ \mu=4}$ (cm^2/s)	64802	7424	8.7	28922	16236	1.8	2.2
$(E_I)_{max,elastic}$ (cm^2/s^2)	32934	7175	4.6	31826	19631	1.6	1.0
$(E_I)_{max,\mu=2}$ (cm^2/s^2)	28990	7367	3.9	26393	16333	1.6	1.1
$(E_I)_{max,\mu=4}$ (cm^2/s^2)	26803	6622	4.0	18935	14634	1.3	1.4

This pulse, characterized by an incremental velocity equal to 200 cm/s, contains most of the seismic energy radiating in the direction of the rupture. As shown in Figure 6c, the maximum of the input energy spectrum occurs at a period of approximately 4.5 s, close to the pulse duration.

In Table 2 the strong ground motion parameters relevant to the FN and FP components of the records considered are reported. Also in this case, the effects of the presence of long-duration pulses in the FN component obtained at Lucerne Valley Station are essentially revealed by velocity and energy parameters (Table 2), with the ratio of the values relevant to the FN component to those relevant to the FP component much greater than unity. Instead, the PGA values are comparable in the FN and FP components of both Lucerne Valley (LV) and Joshua Tree (JT). It is interesting to remark that the ratio of the values relevant to the FN components of the two records examined is close to the unity only in the case of the maximum input energy, $(E_I)_{max}$ (Table 2, last column). However, as shown in Figure 6c, d, while the input energy relevant to JT reaches an isolated narrow peak , centered at a period of about 0.7 s, the values of the spectral ordinate relevant to LV remain considerably high within a large band of periods ($T > 3.0$ s).

Therefore, it can be concluded that the effects of forward directivity conditions are, in this case, more effectively accounted for by the high values of the parameter

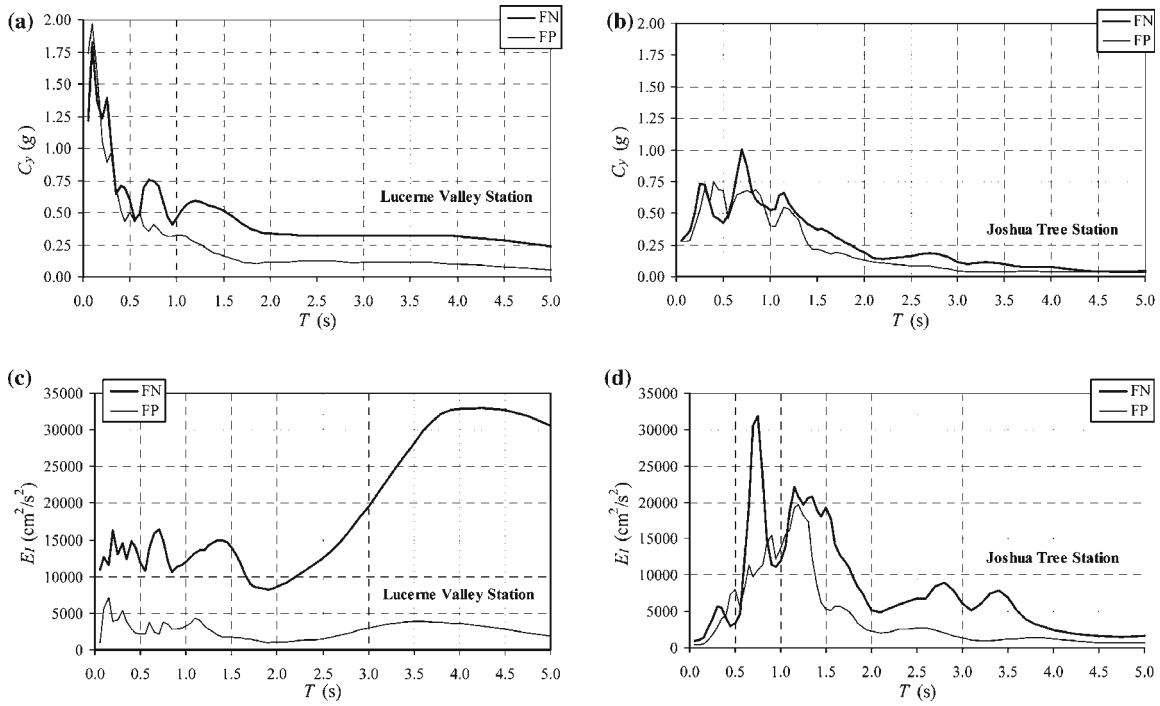

Figure 6. 1992 Landers Earthquake: elastic seismic coefficient, C_y (a, b) and input energy, E_I (c, d) spectra.

AE_I. Finally, in the period range corresponding to the maximum demand in energy terms for LV, i.e., 3–5 s, the values of the spectral ordinates of the seismic coefficient remain close to 0.4 g, and considerably greater than those observed for JT within the same range of periods (Figure 6a, b).

Conditions required for forward directivity are also met in dip slip faulting, including both reverse and normal faults. During the 1994 Northridge earthquake, which occurred on a blind thrust fault, several stations recorded motions affected by rupture directivity effects. The record obtained at Rinaldi Receiving Station (RRS) exhibits significant damage potential due to the presence, in the velocity FN component, of a pulse, occurring after about 2 s from the origin time, with incremental velocity equal to 255 cm/s and duration of 1.2 s. As can be seen from Figure 7b, the peak of E_I is attained at a period of about 1.3 s, approximately equal to the pulse duration. As for 1979, Imperial Valley and 1992, Landers earthquakes, E_I keeps considerably high over a wide range of periods (0.5–2.5 s) and high values of C_y are observed in a similar period range (Figure 7a).

In Figure 8 the time histories of the energy dissipated by hysteresis, E_H, and the displacement demand, δ, are reported for elasto-plastic SDOF systems, with three different natural periods (0.5, 0.7 and 1.3 s), seismic coefficient C_y=0.35 g, and with coefficient, ξ, equal to 5% of the critical damping. Due to the high strength demand, all oscillators yield, and both hysteretic energy and displacement demands do not differ significantly from one oscillator to another. This implies that the seismic input RRS is critical for a broad class of structures.

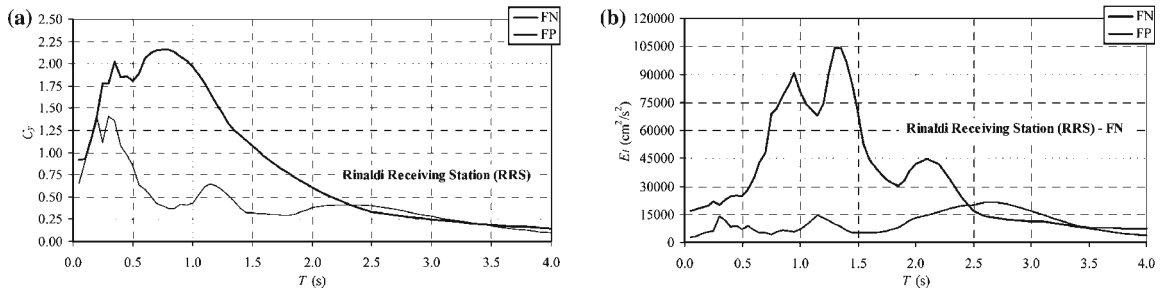

Figure 7. 1994 Northridge Earthquake: elastic seismic coefficient, C_y (a) and input energy, E_I (b) spectra (RRS, FN component).

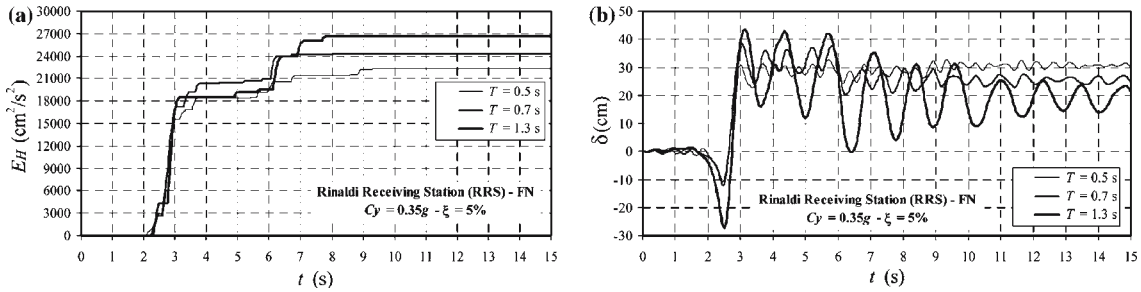

Figure 8. 1994 Northridge Earthquake: hysteretic energy and displacement demands for SDOF systems subject to the seismic input given by the FN component of the Rinaldi Receiving Station record.

4. Characterization of Near-fault Ground Motions

In this study a collection of 252 records obtained during 27 earthquakes has been considered in order to define a series of parameters capable to set the equivalence between idealized and ground motion pulses (Table 3). The selected time histories, recorded at minimum horizontal distances from the surface projection of the causative fault, D_f, not larger than 8–10 km, have been grouped into three magnitude intervals, $5.7 \leqslant M \leqslant 6.2$, $6.5 \leqslant M \leqslant 7.1$, $7.3 \leqslant M \leqslant 7.6$, and, even if for long-duration pulses the influence of the soil stiffness may not be decisive for near-fault records, into three soil classes, indicated as S1, rock or firm soil (70 records), S2, intermediate soil (120 records), S3, soft soil (62 records).

Records included in the data set correspond to different source mechanisms and are representative of fling, forward and backward directivity effects. In Table 4 Mean and Max(imum) values, standard deviation, SD, and coefficient of variation, COV, are reported for peak ground acceleration, PGA, peak ground velocity, PGV, incremental velocity, IV, Housner Intensity, I_H, seismic hazard energy factor, AE_I, and peak energy spectral ordinate, $(E_I)_{max}$, relevant to the FN components of the ground motions listed in Table 3, for the soil classes and magnitude intervals previously defined.

The maximum incremental velocity ranges from 67.1 to 285.4 cm/s, with a not clear dependence on magnitude. Similar considerations apply to the parameter AE_I, with the difference that its lower values always pertain to the interval of the lowest magnitudes, $5.7 \leqslant M \leqslant 6.2$. Anyway, the mean AE_I values appear to increase with M.

Table 3. Earthquakes considered in the present study

No.	Earthquake identification	Year	Month	Day	Hour	Source mechanism	M
1	Imperial Valley, USA	1940	5	19	04:37	Strike slip	7.0
2	Parkfield, USA	1966	6	28	04:26	Strike slip	6.1
3	San Fernando, USA	1971	2	9	14:00	Reverse	6.6
4	Managua, Nicaragua	1972	12	23	06:29	Strike slip	6.2
5	Gazli, Russia	1976	5	17	–	Reverse	6.8
6	Tabas, Iran	1978	9	16	–	Reverse	7.4
7	Coyote Lake, USA	1979	8	6	17:05	Strike slip	5.7
8	Imperial Valley, USA	1979	10	15	23:16	Strike slip	6.5
9	Victoria, Mexico	1980	6	9	03:28	Strike slip	6.4
10	Westmorland, USA	1981	4	26	12:09	Strike slip	5.8
11	Coalinga, USA	1983	5	2	23:42	Reverse-oblique	6.4
12	Nahanni, Canada	1985	12	23	–	Reverse-oblique	6.8
13	North Palm Springs, USA	1986	7	8	09:20	Reverse-oblique	6.0
14	San Salvador	1986	10	10	17:49	Strike slip	5.8
15	Whittier Narrows, USA	1987	10	1	14:42	Reverse	6.0
16	Superstition Hills, USA	1987	11	24	13:16	Strike slip	6.7
17	Loma Prieta, USA	1989	10	18	05:00	Reverse-oblique	6.9
18	Erzican, Turkey	1992	3	13	–	Strike slip	6.9
19	Cape Mendocino, USA	1992	4	25	18:06	Reverse	7.1
20	Landers, USA	1992	6	28	11:58	Strike slip	7.3
21	Northridge, USA	1994	1	17	12:31	Reverse	6.7
22	Kobe, Japan	1995	1	16	20:46	Strike slip	6.9
23	Dinar, Turkey	1995	10	1	15:57	Normal	6.2
24	Umbria-Marche, Italy	1997	9	26	09:40	Normal	6.0
25	Kocaeli, Turkey	1999	8	17	01:51	Strike slip	7.4
26	Duzce, Turkey	1999	11	12	–	Strike slip	7.1
27	ChiChi,Taiwan	1999	9	20	17:47	Reverse	7.6

Energy and displacement demands allow us to characterize the seismic demand in the medium- and long-period range. The large seismic demand imposed by near-fault records is compared with the far-field situation, $D_f \geqslant 10\,\text{km}$, in Figure 9, where mean elastic input energy and displacement spectra are reported. The spectra relevant to far-field conditions were computed for a set of 229 records corresponding to two intervals of D_f, namely $10 \leqslant D_f \leqslant 30\,\text{km}$ and $D_f > 30\,\text{km}$ Decanini and Mollaioli [38].

In a strike-slip earthquake, if the rupture propagates toward the site and the direction of slip on the fault is aligned with the site, forward rupture directivity effects occur, resulting in large values of ground velocity and displacement in the FN directions. The conditions required for forward directivity are also met in dip slip faulting, including both reverse and normal faults. However, not all near-fault locations experience forward rupture directivity effects in a given event. The influence of the FN component, generally resulting in a larger demand imposed to a structural system, is illustrated in Figure 10, where mean elastic input energy and displacement spectra

Table 4. Ground motions parameters

			PGA (cm/s^2)	PGV (cm/s)	IV (cm/s)	I_H (cm)	AE_I (cm^2/s)	$(E_I)_{max}$ (cm^2/s^2)
S1	$5.7 \leqslant M \leqslant 6.2$	Mean	599.5	33.1	50.9	101.6	8377	13883
		SD	149.7	16.7	24.2	55.9	7773	8876
		COV	0.25	0.51	0.48	0.55	0.93	0.64
		Max	873.5	65.8	95.5	192.9	21262	27567
	$6.5 \leqslant M \leqslant 7.1$	Mean	664.6	64.1	94.5	215.2	39424	39206
		SD	332.0	26.7	30.5	80.3	33131	23088
		COV	0.50	0.42	0.32	0.37	0.84	0.59
		Max	1468.9	125.1	151.3	410.1	144282	101014
	$7.3 \leqslant M \leqslant 7.6$	Mean	543.0	66.2	61.6	163.2	36561	21594
		SD	327.5	46.2	17.2	66.2	23922	14291
		COV	0.60	0.70	0.28	0.41	0.65	0.66
		Max	990.8	146.5	85.8	212.5	61864	33413
S2	$5.7 \leqslant M \leqslant 6.2$	Mean	405.4	49.5	73.7	153.5	18256	18684
		SD	140.1	17.0	28.4	56.1	11351	13515
		COV	0.35	0.34	0.39	0.37	0.62	0.72
		Max	667.8	75.8	117.4	240.2	39548	41590
	$6.5 \leqslant M \leqslant 7.1$	Mean	504.7	77.2	109.7	254.9	57797	39583
		SD	171.3	36.4	53.6	103.5	42311	26344
		COV	0.34	0.47	0.49	0.41	0.73	0.67
		Max	827.3	166.0	238.3	457.8	176935	97473
	$7.3 \leqslant M \leqslant 7.6$	Mean	609.8	81.2	120.2	261.7	74528	82287
		SD	265.4	37.6	53.5	114.6	43372	65032
		COV	0.44	0.46	0.45	0.44	0.58	0.79
		Max	949.6	121.1	188.1	466.7	134799	199723
S3	$5.7 \leqslant M \leqslant 6.2$	Mean	303.3	28.6	43.8	112.0	9083	10847
		SD	78.9	17.4	20.3	58.8	7580	3492
		COV	0.26	0.61	0.46	0.53	0.83	0.32
		Max	361.2	48.7	67.1	179.8	17829	14858
	$6.5 \leqslant M \leqslant 7.1$	Mean	443.0	84.1	138.1	291.1	91935	72368
		SD	154.0	22.1	40.8	132.4	61481	51107
		COV	0.35	0.26	0.30	0.45	0.67	0.71
		Max	737.5	127.1	226.6	586.7	252824	205339
	$7.3 \leqslant M \leqslant 7.6$	Mean	537.3	90.4	137.7	274.2	95873	62681
		SD	182.7	40.5	60.6	79.9	70734	35706
		COV	0.34	0.45	0.44	0.29	0.74	0.57
		Max	806.8	176.7	285.4	383.0	225745	121553

are shown, evaluated for $6.5 \leqslant M \leqslant 7.1$ and for three soil types. The diagrams compare the spectra computed for the FN components alone, with those computed for the totality of near-fault records considered in the present study.

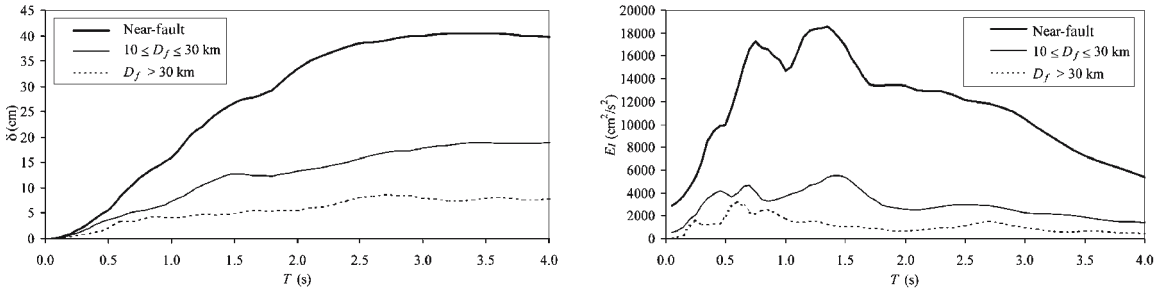

Figure 9. Displacement and energy demands for near-fault and far-field ($D_f \geqslant 10$ km) conditions (soil S2, $6.5 \leqslant M \leqslant 7.1$).

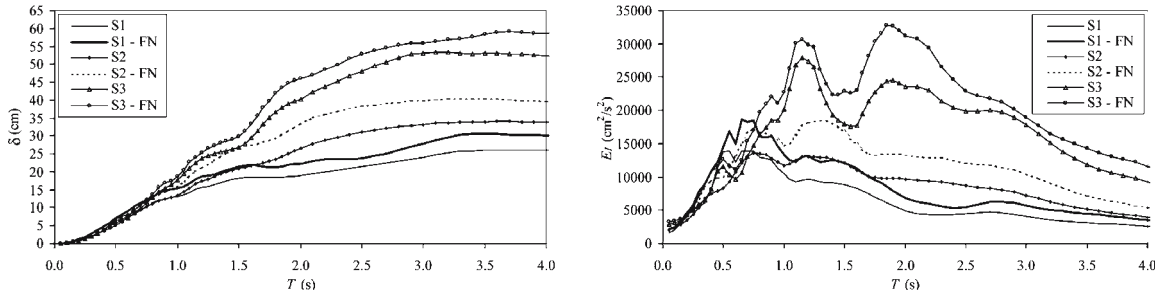

Figure 10. Influence of the fault normal component on the mean elastic displacement, δ, and energy demand, E_I ($6.5 \leqslant M \leqslant 7.1$).

5. Idealized Pulses Equivalent to Near-fault Ground Motions

In order to develop a systematic procedure for the assessment of near-fault effects, near-fault records have been assimilated to simple input pulses that can be fully defined by few but significant parameters. Pulses of various shapes have been investigated for this purpose, and their similarity with a selection of near-fault ground motions is discussed in this section. Following Makris [29], trigonometric functions describing *cycloidal fronts* have been adopted to approximate near-fault pulses, as they constitute differentiable signals resulting in finite acceleration values and allow for simple closed-form solutions. Although cycloidal pulses are able to capture many of the substantial features of the displacement and velocity time histories of near-fault strong ground motions, in many cases the resulting acceleration time histories constitute poor predictions of the recorded ones, since in many near-fault ground motions high-frequency fluctuations may prevail over the long duration pulses. More specifically, type A and B cycloidal pulses may fit ground motions characterized by forward and forward-and-back displacement time histories, respectively, whereas type C_n cycloidal pulses may approximate more complex ground motions exhibiting n main pulses in their displacement histories. Ground velocities relevant to cycloidal pulses of type A and B are respectively expressed as

$$\dot{u}_g^{\mathrm{A}}(t) = \frac{V_p}{2} - \frac{V_p}{2}\cos(\omega_p t), \quad 0 \leqslant t \leqslant T_p \tag{3}$$

$$\dot{u}_g^{\mathrm{B}}(t) = -V_p \cos\left(\omega_p t + \frac{\pi}{2}\right), \quad 0 \leqslant t \leqslant T_p \tag{4}$$

In both expressions, V_p is the amplitude of the velocity pulse and $T_p = 2\pi/\omega_p$ is the period and duration of the pulse.

For type C_n pulses with frequency $\omega_p = 2\pi/T_p$ and duration $T_p^* = (n+1/2)\,T_p - 2\varphi/\omega_p = (n+1/2-\varphi/\pi)\,T_p$, the following definition of ground velocity holds:

$$\dot{u}_g^{C_n}(t) = V_p \sin(\omega_p t + \varphi) - V_p \sin(\varphi),\ 0 \leqslant t \leqslant \left(n + \frac{1}{2} - \frac{\varphi}{\pi}\right) T_p \tag{5}$$

where the value of the phase angle, φ, is determined by requiring that the ground displacement at the end of the pulse be zero, i.e.,

$$\int_0^{(n+1/2-\varphi/\pi)T_p} \dot{u}_g^{C_n}(t)\,dt = 0 \tag{6}$$

For example, for a type C_1 pulse, for which n=1, the solution of this transcendental equation yields φ=0.0697 π. As n increases, a type C_n pulse tends to a harmonic steady-state excitation.

Finally, only for comparison purposes, triangular pulses in velocity have been investigated, here denoted as type T pulses, defined as follows:

$$\dot{u}_g^{T}(t) = \begin{cases} 4V_p t/T_p, & 0 \leqslant t < T_p/4 \\ 2V_p(1-2t/T_p), & T_p/4 \leqslant t < 3T_p/4 \\ 2V_p(1-2t/T_p), & 3T_p/4 \leqslant t \leqslant T_p \end{cases} \tag{7}$$

6. Comparison of the Response to Idealized Pulses and Actual Ground Motions

The equivalence of idealized and recorded pulses has been established on the basis of certain parameters representative of essential features of near-fault ground motions. Thus, on the data set of ground motion records preliminary analyses have been performed in order to identify such parameters. According to the characterization of near-fault ground motions, the appropriate idealized pulse equivalent to a near-fault record has been defined taking into account the comparison of the velocity time histories and the equivalence of the damage potential, expressed in terms of energy. On the one hand, the equivalent velocity pulse has been characterized by means of its duration and severity. While the former quantity is set equal to the period at which a clear peak in the input energy spectrum is attained, i.e. $T_p = T_{(E_I)max}$, the incremental velocity IV appears to be a suitable measure of the latter. On the other hand, the seismic hazard input energy factor AE_I has been used as a measure of the damage potential. A satisfactory correlation exists between IV and the seismic hazard input energy factor. Figure 11 shows, for the elastic case, the trend of the parameter $\sqrt{2AE_I/T_{(E_I)max}}$, representing an equivalent velocity, versus the incremental velocity, IV, for three intervals of magnitude but regardless the soil type.

The regression equations which characterize the correlation of the incremental velocity, IV, the seismic hazard input energy factor, AE_I, and the period corresponding to the maximum spectral ordinate of the input energy, $T_{(E_I)max}$, are expressed as

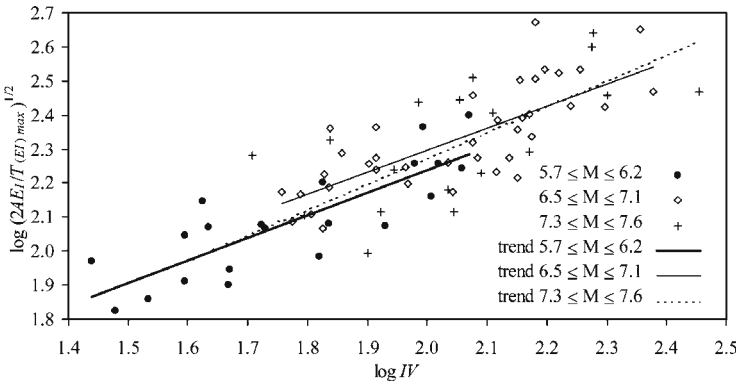

Figure 11. Correlation of IV, elastic AE_I and $T_{(E_I)max}$ for near-fault ground motions.

$$\log\sqrt{2\frac{AE_I}{T_{(E_I)max}}} = \begin{cases} (0.66 \pm 0.10)\log IV + (0.91 \pm 0.18), & r^2 = 0.69,\ 5.7 \leqslant M \leqslant 6.2 \\ (0.65 \pm 0.09)\log IV + (1 \pm 0.19), & r^2 = 0.56,\ 6.5 \leqslant M \leqslant 7.1 \\ (0.75 \pm 0.17)\log IV + (0.76 \pm 0.35), & r^2 = 0.54,\ 7.3 \leqslant M \leqslant 7.6 \end{cases} \tag{8}$$

where r^2 is the correlation coefficient. The adequacy of the prediction, as indicated by the relatively low values of r^2, is affected by the fact that the input energy spectra may present more than one clear peak, and therefore multiple peak values of E_I may be associated to a single value of $T_{(E_I)max}$. The regression lines for the intervals of magnitude $5.7 \leqslant M \leqslant 6.2$ and $6.5 \leqslant M \leqslant 7.1$ are almost parallel, the former remaining constantly below the latter, the regression line for $7.3 \leqslant M \leqslant 7.6$ exhibits a larger slope, perhaps due to the scarce number of records of events with magnitude belonging to that interval.

For the sake of brevity, only the results obtained for the idealized pulses of type B, C_1 and T will be discussed. The following curves approximate the relations existing among AE_I, IV and T_p in the case of elastic behavior, i.e.,

$$\log AE_I = \begin{cases} 2\log IV - 0.09T_p^2 + 0.5T_p - 0.27, & r^2 = 0.99 \text{ (type B pulses)} \\ 2\log IV - 0.09T_p^2 + 0.53T_p - 0.14, & r^2 = 0.99 \text{ (type } C_1 \text{ pulses)} \\ 2\log IV - 0.09T_p^2 + 0.5T_p - 0.45, & r^2 = 0.99 \text{ (type T pulses)} \end{cases} \tag{9}$$

In eqs. (9) the value of the correlation coefficient tends to the unity, as only one energy peak corresponds to a specified duration of the pulse. It is worth noting that eqs. (9) appear to differ in the intercept value only. Figure 12 shows the trend of AE_I versus T_p for a fixed IV (right), and of AE_I versus IV for a fixed T_p (left), for pulses of type B, C_1 and T. AE_I increases with increasing incremental velocity, while, for a specified value of IV, it reaches a maximum and then decreases with increasing pulse duration.

As a general result, equivalent pulses proved to be capable of representing near-fault ground motions within some limitations; the accuracy of such a representation is not equally good in all cases. In order to clarify how the damage potential of near-fault records can be approximated by that described by idealized pulses, two examples will be illustrated in this section. The considered records were obtained from the 1992 Erzincan (Turkey) and 1979 Imperial Valley (California) earthquakes. In the

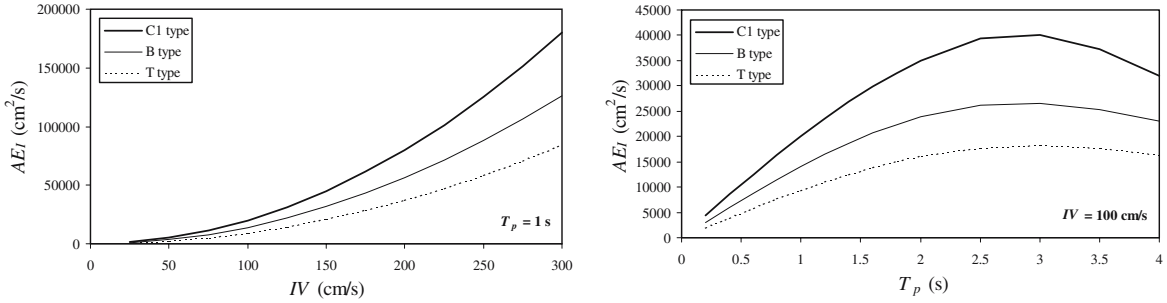

Figure 12. Correlation of elastic IV, AE_I and T_p for idealized pulses of type B, C_1 and T.

first instance, the NS component of the record has been compared with idealized pulses of type B and C_1, the latter providing a better approximation of the velocity time history than the former. The duration of the equivalent idealized pulse has been set equal to the period corresponding to the maximum input energy spectral ordinate, i.e., $T_p = T_{(E_I),max} \cong 2$ s. The severity of the pulse, described by the incremental velocity, has been then determined from the first two of eqs. (9), written for T_p=2 s and for the value of the seismic hazard input energy factor assessed for the Erzincan record, AE_I=74470 cm^2/s. Once the idealized pulses have been determined, acceleration, displacement and input energy spectra have been computed and compared with those evaluated for the strong motion record. In Figure 13, left side, such comparison is illustrated for the elastic displacement demand, δ, and for E_I. The value of the incremental velocity obtained from eqs. (9) for the C_1 type pulse, IV=125 cm/s, is in good agreement with the value obtained from the recorded time history, i.e., 135 cm/s, while a larger value, IV=175 cm/s, is required so that the spectra evaluated for the B type pulse fit those obtained for the Erzincan record. Both idealized pulses appear to provide good approximations of the energy and displacement spectra. However, the spectral accelerations resulting from the idealized pulse are a poor prediction of the recorded values for periods $T < 1.5$ s, i.e. for periods quite smaller than the duration of the idealized pulse itself. The same methodology has been applied to the analysis of the El Centro, array # 6 (Houston Road) record from the 1979 Imperial Valley earthquake. Pulses of type B and C_1 have been taken into account, though the recorded velocity time history appeared to resemble a type B rather than a C_1 pulse. The values $T_p = T_{(E_I)max} \cong$ 3.5 s and AE_I=96560 cm^2/s have been used to derive IV from the first two of eqs. (9). Again, while elastic displacement and energy spectra are accurately predicted by the idealized pulses (Figure 13, right side), idealized and actual acceleration spectra diverge for periods considerably smaller than T_p, i.e. for $T < 2$ s.

The use of idealized pulses seems to produce an adequate characterization of near-fault ground motions also when the inelastic behavior is taken into account. In Figure 14, δ and AE_I are shown for elastoplastic SDOF systems and two values of the displacement ductility, μ. In both cases, the spectra relevant to the Erzincan record appear to be accurately approximated by the appropriate pulse of type C_1, actually some improvement in the prediction of the spectral acceleration ordinates is obtained, in comparison with the elastic case.

For the evaluation of elastic and inelastic response of multi-story frame structures [27, 41] the comparison has been extended to MDOF systems, using an equivalent

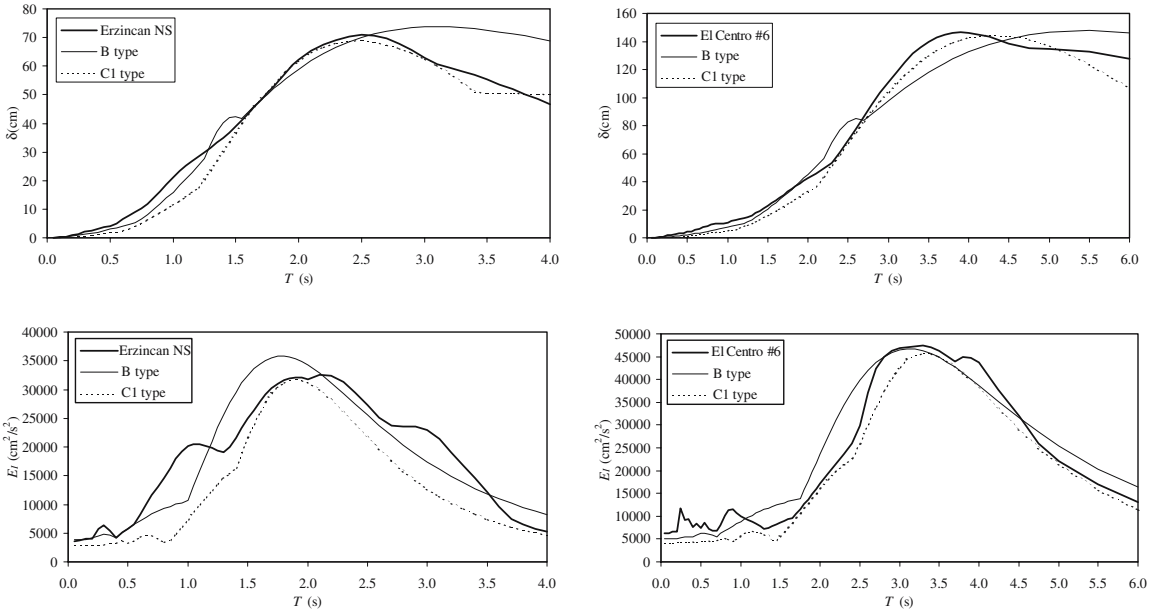

Figure 13. Idealized pulses and near-fault ground motions: comparison of elastic spectra.

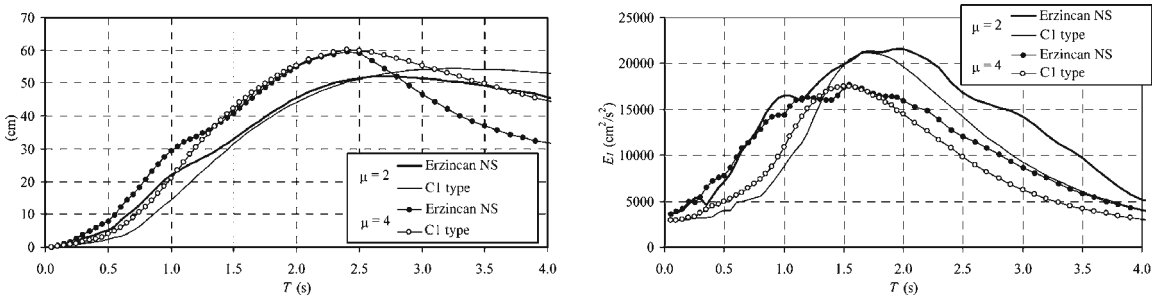

Figure 14. Idealized pulses and near-fault ground motions: comparison of inelastic spectra.

discrete shear-type model, denoted as ESTM model. The choice of a simplified model, whose effectiveness is validated by comparing the results with those derived from more detailed non-linear time histories analyses, permits to take into account all the vibration modes that implicitly contribute to the seismic response, and to define response spectra of local demands, such as the interstory drift.

Ten different multi-story structural systems have been modeled using two-dimensional, two-bay generic frames with constant story height and beam spans. The number of stories varies from 2 to 24 in order to simulate a significant range of typologies of reinforced concrete buildings. A realistic, approximately parabolic, stiffness distribution with full constraint for the joints at the base of the columns has been assumed for each selected frame. A stiffness-degrading hysteretic model has been adopted for the cyclic behavior of the frames in each story. The yielding strengths of the stories have been obtained by an inverted-triangular distribution of equivalent seismic forces, with an additional force at the top of buildings having fundamental periods larger than 0.7 s.

The analysis on a set of frames, characterized by a wide range of vibration periods, allows the characterization of inter-story drift spectra, where the maximum

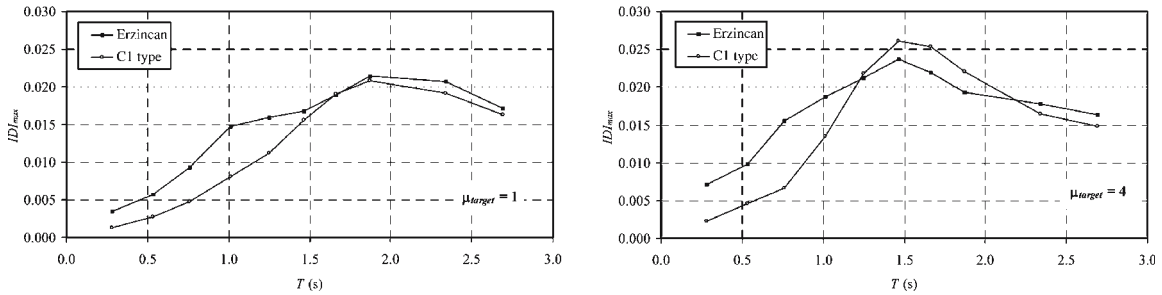

Figure 15. Idealized pulse and near-fault ground motion: comparison of interstory drift spectra.

inter-story drift IDI_{max}, defined as the maximum inter-story displacement normalized by the story height, is represented. As an example, Figure 15 illustrates the comparison of the inter-story drift spectra relevant to Erzincan record and to a pulse of type C_1 (T_p=1 s) for target maximum ductility ratios μ_{target}=1 (elastic) and μ_{target}=4. The quantity μ_{target} has been set from constant ductility inelastic strength demand spectra of SDOF systems equivalent to MDOF systems of assigned mechanical properties [41]. As in the case of SDOF systems, the comparison reveals notable resemblances between the response to the record and the response to the synthetic pulse, particularly in the frequency range around the period of the pulse. These consistent similarities, between MDOF response to near-fault ground motions in forward directivity and that to the idealized pulses, support the argument that near-fault records can indeed be represented by equivalent idealized pulses.

7. Conclusions

The paper is focused on the characterization of the damage potential of long-period pulses, recorded in near-fault and forward directivity conditions, during recent earthquakes. The effects of pulse-type ground motions have been analyzed by computing yield strength, C_y, energy, AE_I, and displacement, δ, demand for elastic and inelastic SDOF systems subjected to long period pulses, and underlining the differences with respect to the response behavior to high frequency signals. The results confirm that, while the linear-elastic response of a structural system is controlled by the resonance phenomenon, considerably larger deformations can be induced by long duration pulses with effective accelerations even slightly greater than that corresponding to the yielding strength of the structure.

Many near-fault ground motions, classified according to soil type and interval of magnitude, are the basis for the identification of a set of parameters adequately correlated with the seismic damage potential. These parameters are thus suitable to establish the equivalence between idealized and real ground motion pulses. In addition to conventional response spectra, elastic and inelastic spectra of input energy, hysteretic energy, displacement and seismic yield strength, synthetic parameters derived from the strong ground motion records and taking into account simultaneously the amplitude, duration and number of cycles of the near-fault pulse are evaluated. Velocity and energy-based parameters appear to correlate adequately

well with the faulting and wave propagation processes, and therefore to constitute appropriate indicators of the effects of near-fault pulses, especially in forward directivity conditions. A particularly satisfactory degree of correlation exists between the incremental velocity and the seismic hazard energy factor.

Starting from an energy-based characterization of the damage potential, the appropriate idealized pulse, represented by trigonometric functions, is defined taking the equivalence of the near-fault velocity time histories and of the damage potentials expressed in terms of energy into account. While the equivalent velocity pulse is characterized by means of its duration – represented by the period at which a clear peak in the input energy spectrum is attained – and severity – quantified by the incremental velocity – the seismic hazard energy factor, AE_I, is used as an index of the damage potential.

Equivalent pulses are capable of representing the salient features of the response to near-fault ground motions. In particular, as far as displacement and input energy spectra are concerned, response quantities to idealized pulses constitute a good approximation of those computed using recorded ground motions, both for the elastic and inelastic behavior of SDOF and MDOF systems. Differences are instead detected in the acceleration spectra, though in the range of relatively high frequencies only.

The proposed methodology provides a straightforward yet dependable mathematical model which allows us to select, for a certain structural system, the critical pulse-type motion as a function of the magnitude, and to study the dynamic structural response to simplified waveforms that capture the time history and response spectra characteristics of near-fault recorded ground motions.

References

1. Bolt, B.A. and Abrahamson, N.A., 'Estimation of strong ground motion', *International Handbook of Earthquake Engineering Seismology*, IASPEI, 2003.
2. Somerville, P., Irikura, K., Graves, R., Sawada, S., Wald, D., Abrahamson, N., Iwasaki, Y., Kagawa, T., Smith, N. and Kowada, A., 'Characterizing earthquake slip models for the prediction of strong ground motions', *Seismol. Res. Lett.* **70**(1), (1998) 59–80.
3. Somerville, P.G., 'Magnitude scaling of the near fault rupture directivity pulse', *Proceedings of the International Workshop on the quantitative prediction of strong-motion and the Physics of Earthquake sources*, 23–25 October 2000, Tsukuba, Japan, 2001.
4. Bolt, B.A., Irikura, K., Panza, G.F. and Saragoni, R., 'Seismic ground motion assessment and realistic modeling for base-isolated structures', *Proceedings of the 8th World Seminar on Seismic isolation, Energy dissipation and Active vibrations Control of Structures*, 4–10 October 2003, Yerevan, Armenia.
5. Somerville, P.G., 'Seismic hazard evaluation', *Proceedings of the 12th World Conference on Earthquake Engineering*, Auckland, New Zealand, 30 January – 4 February 2000, Paper No. 2833, New Zealand Society for Earthquake Engineering, Silverstream, Upper Hutt, NZ.
6. Somerville, P.G. and Graves, R.W., 'Conditions that give rise to unusually large long period ground motions', *Proceedings of the Seminar on Seismic Isolation, Passive Energy Dissipation and Active Control*, Applied Technology Council, San Francisco, ATC17-1, **1** (1993) 83–94.
7. Somerville, P.G., Smith, N.F., Graves, R.W. and Abrahamson, N.A., 'Modification of empirical strong ground motion attenuation relations to include the amplitude and duration effects of rupture directivity', *Seismol. Res. Lett.* **68**(1) (1997) 199–222.

8. Bertero, V.V., Herrera, R.A and Mahin, S.A., 'Establishment of design earthquake – evaluation of present methods', *Proceedings of the International Symposium on Earthquake Structural Engineering*, St. Louis, Mo., 1, 1976, pp.551–580.
9. Bertero, V.V., Herrera, R.A and Mahin, S.A., 'Aseismic design implications of near-fault San Fernando Earthquake records', *Earthquake Eng. Struct. Dyn.* **6** (1978) 31–42.
10. Archuleta, R.J. and Hartzell, S.H., 'Effects of fault finiteness on near-source ground motion', *Bull. Seismol. Soc. Am.* **71**(4) (1981) 939–957.
11. Panza, G. F. and Suhadolc, P., 'Complete strong motion synthetics, In: Bolt B.A. (ed), *Seismic Strong Motion Synthetics*', Academic Press, New York, 1987, pp.153–204.
12. Abrahamson, N.A. and Somerville, P.G., 'Effects of the Hanging Wall and footwall on ground motions recorded during the Northridge Earthquake', *Bull. Seismol. Soc. Am.* **86**(1B) (1996) S93–S99.
13. Bertero, V.V., Anderson, J.C. and Sasani, M., 'Impulse earthquake ground motions: a historical and critical review, *Proceedings of the 1999 ASCE Structures Congress*', ASCE, Reston, VA, 1999, pp. 91–94.
14. Mavroedis, G.P. and Papageorgiou, A.S., 'A mathematical representation of near-fault ground motions', *Bull. Seismol. Soc. Am.* **93**(3) (2003) 1099–1131.
15. Decanini, L.D. and Prato, C.A., *Proyecto de Reglamento CIRSOC 103: Accion de los sismos sobre las construcciones*, Centro de Investigacion de los Reglamentos Nacionales de Seguridad para las Obras Civiles, Argentina, 1980.
16. *Uniform Building Code*: *Structural Engineering Design Provisions (UBC)*, International Conference of Building Officials (ICBO), Whittier, CA, 1997.
17. Bolt, B.A., *From Earthquake Acceleration to Seismic Displacement*, The Fifth Mallet-Milne Lecture, SECED, John Wiley & Sons, Chichester, England, 1996.
18. Anderson, J.C. and Bertero, V.V., 'Uncertainties in establishing design earthquakes', *ASCE J. Struct. Eng.* **113**(8) (1987) 1709–1724.
19. Naeim, F., 'On seismic design implications of the 1994 Northridge earthquake records', *Earthquake Spectra* **11**(1) (1995) 91–109.
20. Decanini, L.D. and Mollaioli, F., 'Parameters to be considered in the establishment of the design earthquake based on energy concepts', *Proceedings of the Structural Engineers World Congress*, San Francisco, CA, Paper No T227–5, 1998a.
21. Hall, J.F., Heaton, T.H., Halling, M.W. and Wald, D.J., 'Near-source ground motion and its effects on flexible buildings', *Earthquake Spectra*, **11**(4) (1995) 569–605.
22. Iwan, W.D., 'Drift spectrum: measure of demand for earthquake ground motions', *ASCE J. Struct. Eng.* **123**(4) (1997) 397–404.
23. Baez, J.I. and Miranda, E., 'Amplification factors to estimate inelastic displacement demands for the design of structures in the near field', *Proceedings of the 12th World Conference on Earthquake Engineering*, Auckland, New Zealand, 30 January – 4 February 2000, Paper No. 1561, New Zealand Society for Earthquake Engineering Silverstream, Upper Hutt, NZ, 2000.
24. Chopra, A.K. and Chintanapakdee, C., 'Comparing response of SDF systems to near-fault and far-fault earthquake motions in the context of spectral regions', *Earthquake Eng. Struct. Dyn.* **30** (2001) 1769–1789.
25. MacRae, G.A., Morrow, D.W. and Roeder, C.W., 'Near-fault ground motion effects on simple structures', *ASCE J. Struct. Eng.* **127**(9) (2001) 996–1004.
26. Akkar, S. and Gulkan, P., 'A critical examination of near-field accelerograms from the Sea of Marmara Region earthquakes', *Bull. Seismol. Soc. Am.* **92**(1) (2002) 428–447.
27. Decanini, L.D., Mollaioli, F. and Mura, A., 'Shear-beam model for the prediction of the response of MDOF systems subjected to severe earthquake ground shaking', *Proceedings of the 12th European Conference on Earthquake Engineering*, London, 9–13 September 2002, Paper No. 055, 2002.
28. Alavi, B. and Krawinkler, H., 'Behavior of moment-resisting frame structures subjected to near-fault ground motions', *Earthquake Eng. Struct. Dyn.* **33** (2004) 687–606.
29. Makris, N., 'Rigidity–plasticity–viscosity: can electrorheological dampers protect base-isolated structures from near-source ground motions?', *Earthquake Eng. Struct. Dyn.* **26** (1997) 571–591.

30. Malhotra, P.K., 'Response of buildings to near-field pulse-like ground motions', *Earthquake Eng. Struct. Dyn.*, **28** (1999) 1309–1326.
31. Cuesta, I. and Aschheim, M.A., 'Isoductile strength and strength reduction factors of elasto-plastic SDOF systems subjected to simple waveforms', *Earthquake Eng. Struct. Dyn.* **30** (2001) 1043–1059.
32. Menun, C. and Fu, Q., 'An analytical model for near-fault ground motions and the response of MDOF systems', *Proceedings of the 12th European Conference on Earthquake Engineering*, London, 9–13 September 2002, Paper No. 647.
33. Mollaioli, F., Decanini, L.D. and Bruno, S., 'Damage potential of severe long duration acceleration pulses in near-fault records', *Proceedings of the 12th European Conference on Earthquake Engineering*, London, 9–13 September 2002, Paper No. 155, 2002.
34. Bray, J.D. and Rodriguez-Marek, A., 'Characterization of forward-directivity ground motions in the near-fault region', *Soil Dyn. Earthquake Eng.* **24** (2004) 815–828.
35. Decanini, L.D., Mollaioli, F. and Saragoni, R., 'Energy and displacement demands imposed by near-source ground motions', *Proceedings of the 12th World Conference on Earthquake Eng.*, Auckland, New Zealand, 30 January – 4 February 2000, Paper No. 1136, New Zealand Society for Earthquake Engineering Silverstream, Upper Hutt, NZ, 2000.
36. Mollaioli, F. and Decanini, L.D., 'Influenza delle pulsazioni accelerometriche di lunga durata sui danneggiamenti osservati in recenti terremoti', *Proceedings of the VIII Convegno Nazionale ANIDIS "L'Ingegneria sismica in Italia"*, Taormina, 21–24 September 1997, **2**, pp.1269–1278 (in Italian).
37. Uang, C.M. and Bertero, V.V. (1990), 'Evaluation of seismic energy in structures', *Earthquake Eng. Struct. Dyn.* **19** (1990) 77–90.
38. Decanini, L.D. and Mollaioli, F., 'Formulation of elastic earthquake input energy spectra', *Earthquake Eng. Struct. Dyn.* **27** (1998b) 1503–1522.
39. Housner, G.W., 'Spectrum intensities of strong motion earthquakes', *Proceedings of the Symposium of Earthquake and Blast Effects on Structures*, EERI, Los Angeles, California, 1952, pp. 21–36.
40. Uang, C.M. and Bertero, V.V., '*Implications of recorded earthquake ground motions on seismic design of building structures*', Report No. UCB/EERC-88/13, Earthquake Engineering Research Center, College of Engineering, University of California at Berkeley, 1988.
41. Decanini, L.D., Mollaioli, F. and Mura, A., 'Simplified shear-type model for the evaluation of the influence of ductility and stiffness distribution patterns on multi-story structures', *Proceedings of the 11th Italian National Conference "L'ingegneria Sismica in Italia"*, Genova, Italy, 25–29 January 2004, Paper No. D1–01.